

Supplementary Information

Achieving High Capacity and Long Cycling Life in Aqueous Zinc-Sulfur Batteries with Improved Kinetics through Electrolyte Solvation Engineering

Tino S. Thomas, Aayushi Prakash Sinha, Debaprasad Mandal*

Department of Chemistry, Indian Institute of Technology Ropar, Punjab 140001, India

Materials

Sulfur powder and Zn foil (0.5 mm thickness) were received from Thermo Fischer Scientific whereas, zinc triflate ($\text{Zn}(\text{OTf})_2$) was obtained from TCI, N, N-Dimethylformamide (DMF), Acetonitrile (ACN), Dimethylsulfoxide (DMSO) was obtained from Spectrochem and zinc iodide (ZnI_2) were procured from Sigma Aldrich. Ketjen black (KB) and PVDF were obtained from the Electrode Store. All electrolytes were prepared using de-ionized water with a resistivity of 18 $\text{M}\Omega$, and all the above reagents were analytically pure grade and were used without further purification.

Measurements and Characterization

Powder X-ray diffraction (PXRD) measurements were conducted using PANalytical X'PERT pro diffractometer using $\text{Cu-K}\alpha$ radiation ($\lambda=0.1542$ nm, 20 kV, 20 mA) in the 2θ range from 5 to 80° with a scan speed of $10^\circ/\text{min}$. Bruker Tensor-27 with a zinc selenide window was used for recording FT-IR spectra ranging from 4000 to 400 cm^{-1} . The water contact angle was determined using a Kyowa DMe-211 Plus by the sessile water drop method at ambient temperature. X-ray photoelectron spectroscopy (XPS) was conducted to identify the various oxidation states and species formed using Thermo Fisher Scientific Escalab Xi^+ spectrometer with a monochromatic $\text{Al K}\alpha$ radiation (1486.6 eV). Morphological analysis of materials and electrodes was done using field emission scanning electron microscopy (FESEM) using JEOL JSM-7610F. Optical images of electrodes before and after cycling were recorded using an Olympus microscope. ^1H NMR spectra of the electrolytes were recorded using a JEOL JNM-ECS 400 MHz spectrometer at ambient probe temperatures with δ -acetone serving as the internal reference. Raman spectra was acquired using LabRAM HR Evolution (Horiba Scientific) in the range of 100 cm^{-1} - 500 cm^{-1} using a 532 nm laser as the excitation source.

Electrochemical measurements

Sulfur was physically ground with activated carbon in a 1:1 mass ratio followed by the melt diffusion under inert conditions at 155°C for 12 h. The solid obtained was allowed to cool down to room

temperature and denoted as S@AC. The sulfur cathode for all electrochemical measurements was then prepared by mixing S@AC, Ketjen Black (KB), and PVDF in a weight ratio of 8:1:1 in N-Methyl-2-pyrrolidone (NMP). The slurry was then ultrasonicated and the mixed slurry was uniformly coated on a graphite sheet (10 mm dia.) with sulfur loading between 1.3-1.5 mg cm⁻². The cathodes were dried in a vacuum oven at 60 °C for 12 h. For the Swagelok cell assembly, zinc foil with a diameter of 10 mm served as an anode, and GF-D glass fiber served as a separator. Different electrolytes containing 2M Zn(OTf)₂ in water (denoted as AZ) were prepared as follows: AZ, AZ/ZnI₂, and AZ/ACN (x%)/ZnI₂, where x% represents ACN in a weight ratio of 20%, 40%, and 60% respectively with 0.05 wt.% ZnI₂ added in all the electrolytes; AZ, AZ/ZnI₂, and AZ/DMF (x%)/ZnI₂, where x% represents DMF in a weight ratio of 20%, 30%, and 40% respectively; and AZ, AZ/ZnI₂, and AZ/DMSO (x%)/ZnI₂, where x% represents DMSO in a weight ratio of 10%, 20%, 30%, and 40% respectively. 60 µL electrolytes were used in all battery studies. Linear sweep voltammetry (LSV) and electrochemical impedance (EIS) were carried out using glassy carbon (3 mm), Ag/AgCl/3M KCl, and Pt wire as the working, reference, and counter electrode respectively using Metrohm Autolab M204. Linear polarization was performed using zinc foil as a working electrode at 1 mV s⁻¹ scan rate from -0.3 V to +0.3 V vs OCP whereas, the electrochemical impedance spectroscopy (EIS) was recorded from 1 MHz to 0.1 Hz. Cyclic voltammetry (CV) was performed to assess nucleation overpotential (NOP) by scanning from 0 V to -1.5 V at 50 mV s⁻¹ using graphite sheet as working, Ag/AgCl/3M KCl as reference, and Zn foil as counter electrodes. Zn²⁺ diffusion curves were obtained via chronoamperometry (CA) in Zn||Zn symmetric cells under an overpotential of -150 mV. All batteries were rested overnight before cycling at ambient conditions. The galvanostatic charge-discharge (GCD) profile of Zn//Zn symmetrical cells and Zn/S batteries, cyclic voltammetry, and electrochemical impedance spectroscopy (EIS) were performed using the battery cycler (BCS-810, Biologic) at ambient conditions. Galvanostatic intermittent titration technique (GITT) measurements were performed with a cutoff voltage of 1.5-0.1 V (vs. Zn²⁺/Zn). A constant current density of 0.1 A g⁻¹ was applied for 1 h, followed by a relaxation step of 2 h until the voltage reached upper or lower limits. The diffusion coefficient (D) was obtained using the following equation:

$$D = \frac{4}{\pi\tau} \left(\frac{m_B V_M}{M_B A} \right)^2 \left(\frac{\Delta E_s}{\Delta E_\tau} \right)^2$$

where τ is the duration time of the discharge step, m_B is the mass of active material, M_B and V_M are the molecular weight and molar volume of sulfur, respectively, A is the contact area between electrode and electrolyte, ΔE_τ is the change of cell voltage during discharge, ΔE_s is the change of steady-state voltage for the corresponding step.

Computational methods

DFT calculations were performed with the Gaussian 09W software package to gain structural information on the solvation ions. The geometries of all species were fully optimized without any symmetry constraint at the B3LYP level of theory by considering the water solvation effect in the CPCM model. In these calculations, we used Hay-Wadt effective core potentials (ECPs) with the associated Lanl2dz basis set for Zn and the standard 6-31G+(d, p) basis set for all other atoms.

The adsorption energy (E_{ads}) is defined as

$$E_{\text{ads}} = E_{\text{Zn-solvent}} - E_{\text{Zn}} - E_{\text{solvent}}$$

where $E_{\text{Zn-solvent}}$ is the total DFT energy of the optimized structure and E_{Zn} and E_{solvent} are the energies of the Zn ion and the solvent, respectively.

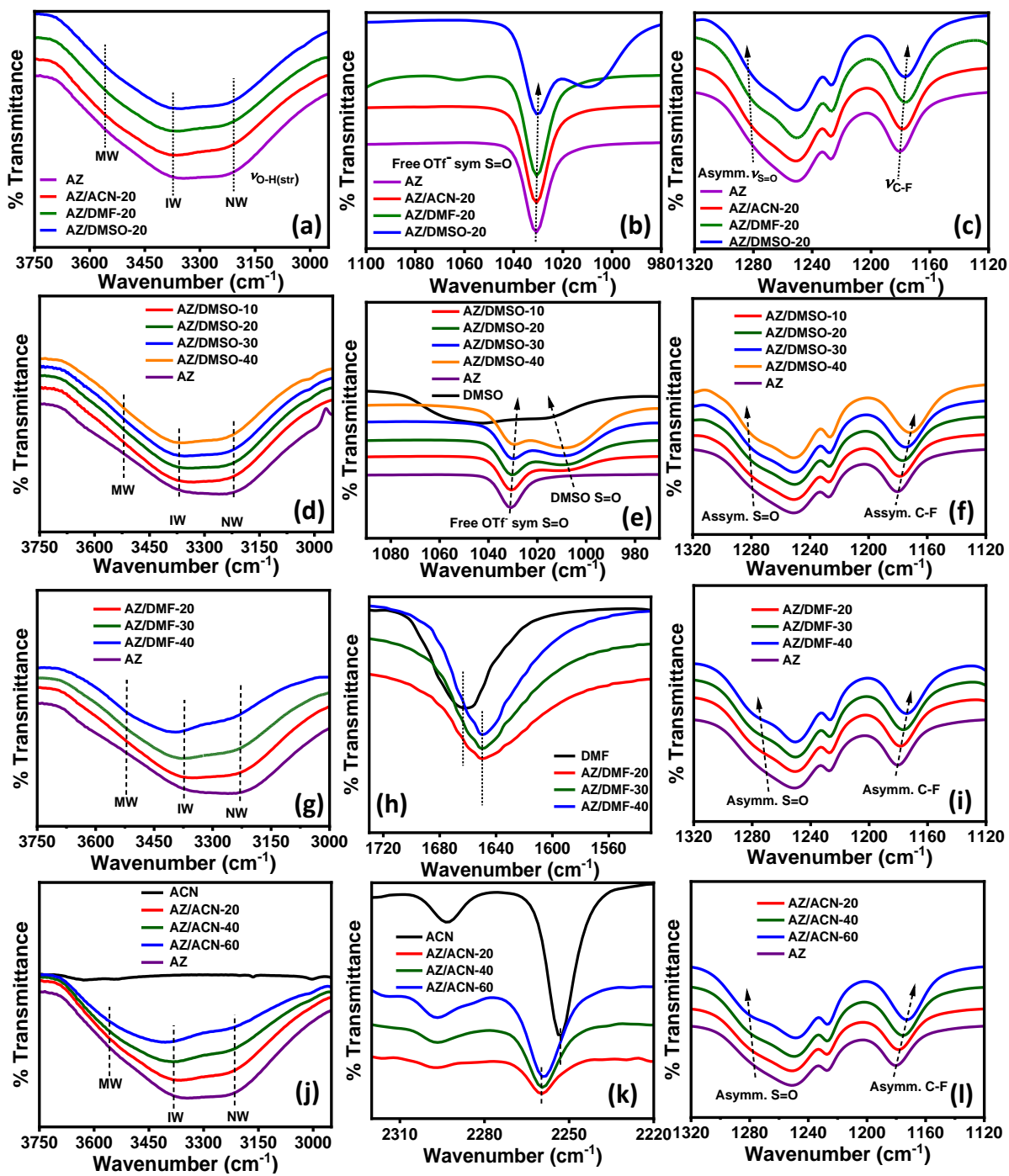


Fig. S1. FT-IR spectra of (a-c) AZ, ACN-20, DMF-20, and DMSO-20; (d-f) AZ, DMSO-10, DMSO-20, DMSO-30, and DMSO-40; (g-i) AZ, DMF-20, DMF-30, and DMF-40; (j-l) AZ, ACN-20, ACN-40, and ACN-60 electrolytes.

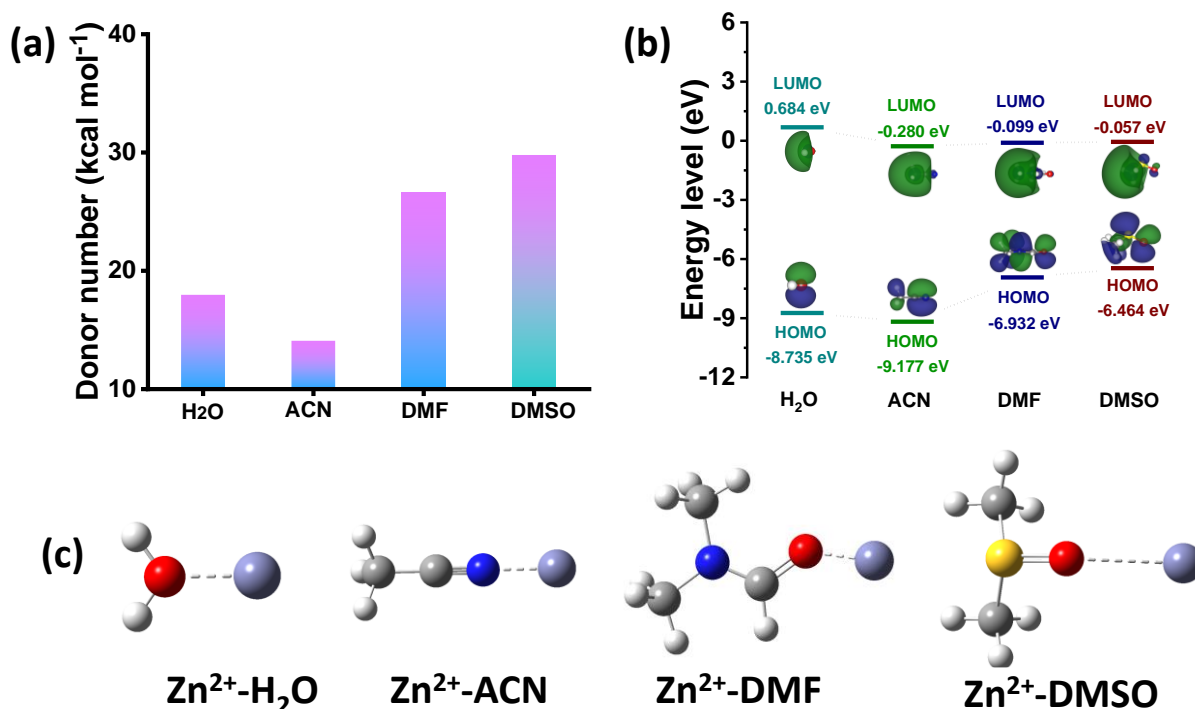


Fig. S2. (a) Donor number of various solvents; (b) HOMO and LUMO energy level of these solvents, and (c) Optimized structure of Zn²⁺-additive complex (Colour code: Zn²⁺: gray; N: blue; O: red; S: yellow)

Molecular orbital calculations were conducted to determine the affinity of solvents towards zinc ions, focusing on the energy levels of the lowest unoccupied molecular orbital (LUMO) and highest occupied molecular orbital (HOMO), summarized in Fig. 2g. Based on molecular orbital theory, a narrow HOMO-LUMO band gap indicates enhanced electron transfer capability i.e. facile electron transfer onto zinc thereby facilitating solvent adsorption onto the metal surface. The calculated band gaps for water, ACN, DMF, and DMSO were 9.419, 8.897, 6.833, and 6.407 eV, respectively. These findings reveal that DMF and DMSO exhibit significantly narrower band gaps and superior adsorption energies than water and ACN, highlighting their effectiveness in interacting with the zinc surface.

Table S1. HER overpotential obtained from LSV of various electrolytes by varying concentrations of ACN.

Electrolyte	HER overpotential (V)
ACN-0	-0.99
ACN-20	-1.02
ACN-40	-1.06
ACN-60	-1.07

Table S2. HER overpotential obtained from LSV of various electrolytes by varying concentrations of DMF.

Electrolyte	HER overpotential (V)
DMF-0	-0.99
DMF-20	-1.06
DMF-30	-1.08
DMF-40	-1.10

Table S3. HER overpotential obtained from LSV of various electrolytes by varying concentrations of DMSO.

Electrolyte	HER overpotential (V)
DMSO-0	-0.99
DMSO-10	-1.07
DMSO-20	-1.09
DMSO-30	-1.14
DMSO-40	-1.27

Table S4. Electrochemical parameters obtained from EIS for different concentrations of ACN.

Electrolyte	R_s ($\Omega \text{ cm}^2$)	R_{ct} ($\Omega \text{ cm}^2$)
ACN-20	2.3	11.9
ACN-40	3.1	12.2
ACN-60	5.4	15.6

Table S5. Electrochemical parameters obtained from EIS for different concentrations of DMF.

Electrolyte	R_s ($\Omega \text{ cm}^2$)	R_{ct} ($\Omega \text{ cm}^2$)
DMF-20	7.9	12.1
DMF-30	15.5	12.7
DMF-40	20.7	13.1

Table S6. Electrochemical parameters obtained from EIS for different concentrations of DMSO.

Electrolyte	R_s ($\Omega \text{ cm}^2$)	R_{ct} ($\Omega \text{ cm}^2$)
DMSO-10	7.3	11.9
DMSO-20	12.1	12.3
DMSO-30	23.8	12.6
DMSO-40	30.3	13.3

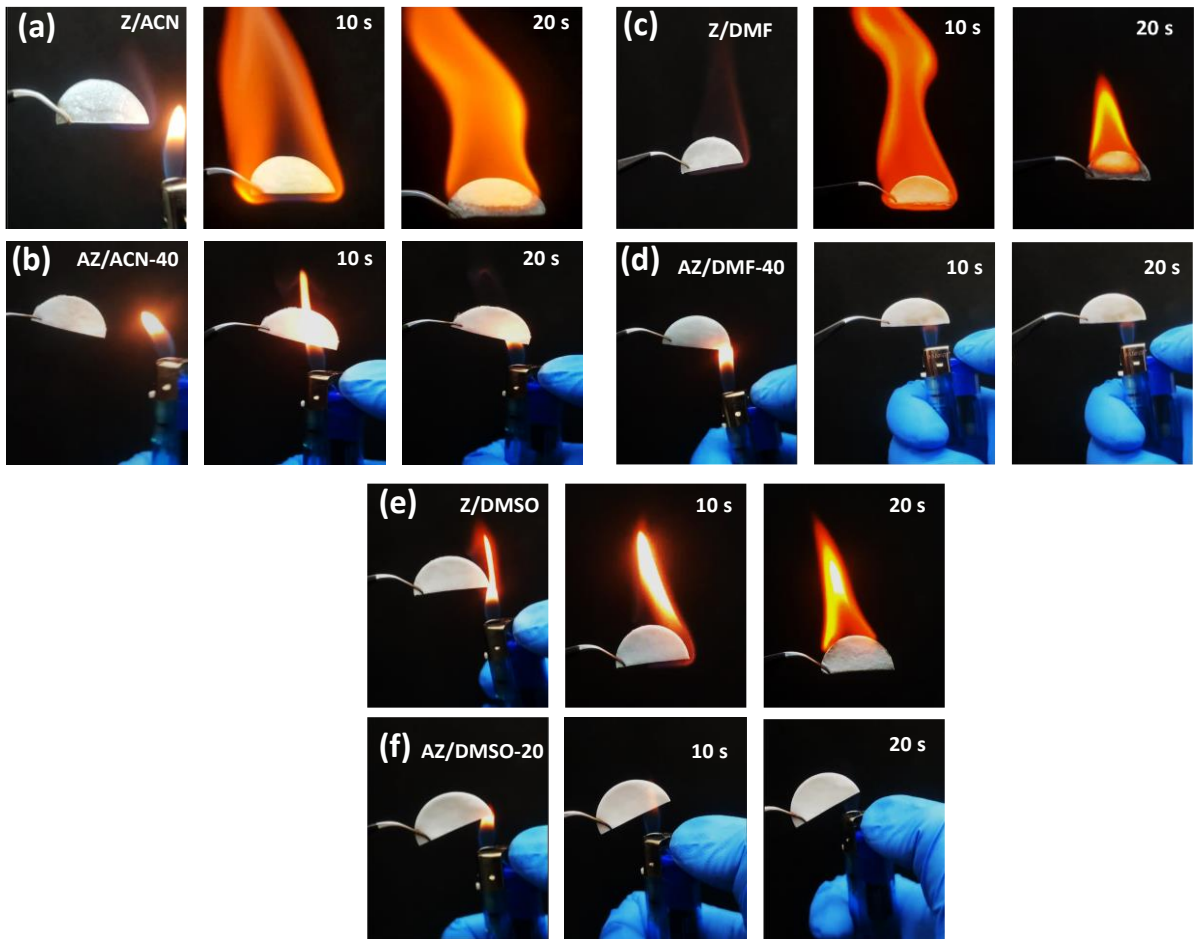


Fig. S3. Flammability test of separator soaked in (a) Z/ACN/ZnI₂; (b) AZ/ACN-40/ZnI₂; (c) Z/DMF/ZnI₂ electrolytes; (d) AZ/DMF-40/ZnI₂; (e) Z/DMSO/ZnI₂, and (f) AZ/DMSO-20/ZnI₂ electrolytes (in 2M Zn(OTf)₂).

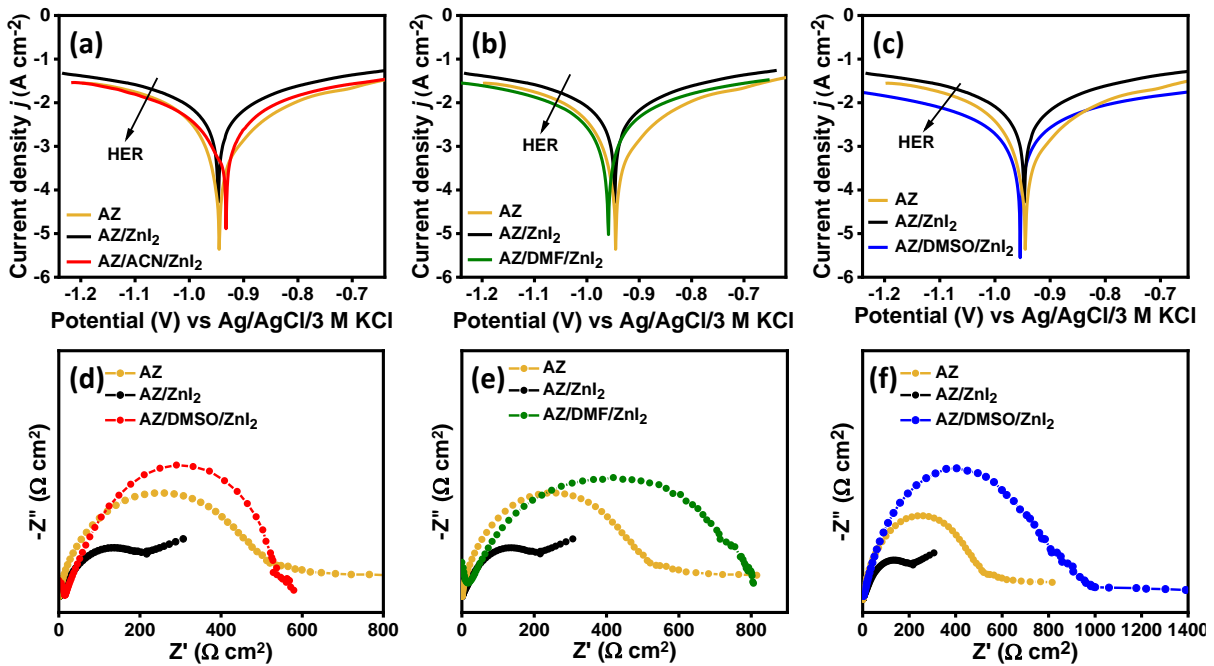


Fig. S4. Linear polarization of (a) ACN, (b) DMF, and (c) DMSO based electrolytes at a scan rate of 1 mV s⁻¹; Corresponding EIS spectra of (d) ACN, (e) DMF, and (f) DMSO based electrolytes using zinc foil, Ag/AgCl/3 M KCl and Pt wire as working, reference, and counter electrodes, respectively.

Table S7. Electrochemical parameters obtained from potentiodynamic linear polarization curves for Zn anodes in aqueous and ACN-based hybrid electrolytes.

Electrolyte	E_{corr} (V)	I_{corr} (mA cm ⁻²)	Corrosion rate (mm y ⁻¹)
AZ	-0.94	4.3	52.6
AZ/ZnI ₂	-0.94	12.6	371.8
AZ/ACN/ZnI ₂	-0.93	3.8	116.3

Table S8. Electrochemical parameters obtained from potentiodynamic linear polarization curves for Zn anodes in aqueous and DMF-based hybrid electrolytes.

Electrolyte	E_{corr} (V)	I_{corr} (mA cm ⁻²)	Corrosion rate (mm y ⁻¹)
AZ	-0.94	4.3	52.6
AZ/ZnI ₂	-0.94	12.6	371.8
AZ/DMF/ZnI ₂	-0.96	3.4	97.9

Table S9. Electrochemical parameters obtained from potentiodynamic linear polarization curves for Zn anodes in aqueous and DMSO-based hybrid electrolytes.

Electrolyte	E_{corr} (V)	I_{corr} (mA cm ⁻²)	Corrosion rate (mm y ⁻¹)
AZ	-0.94	4.3	52.6
AZ/ZnI ₂	-0.94	12.6	371.8
AZ/DMSO/ZnI ₂	-0.95	2.6	60.1

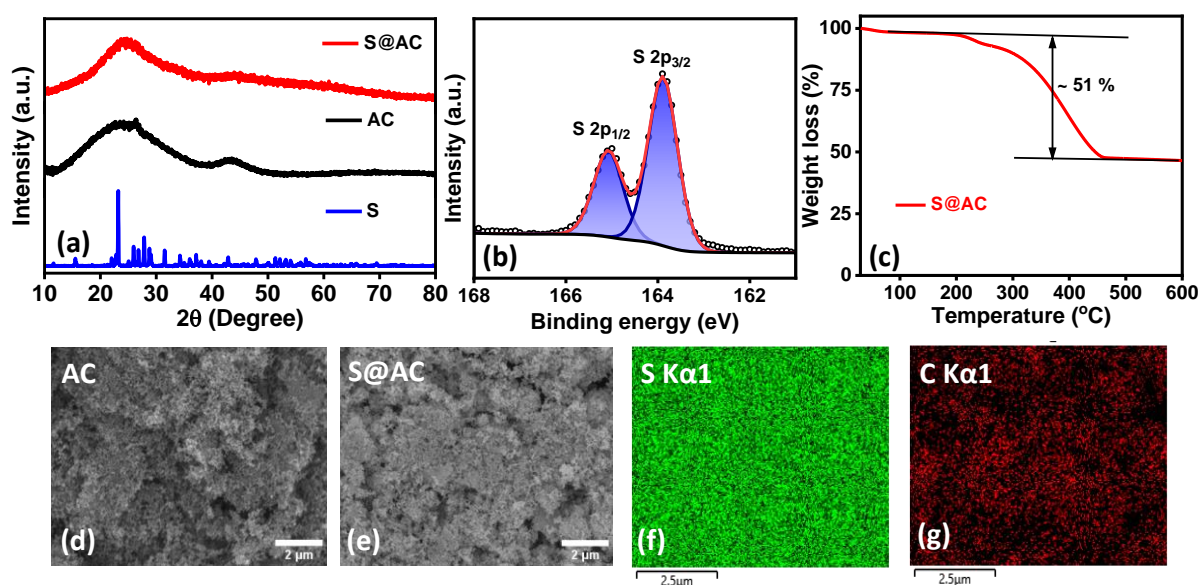


Fig. S5. (a) PXR D of pure S, AC, and S@AC; (b) Deconvoluted S2p XPS spectrum; (c) TGA of the S@AC composite; FESEM images of (d) AC; (e) S@AC; Elemental dot mapping of (f) carbon, and (g) sulfur of S@AC composite.

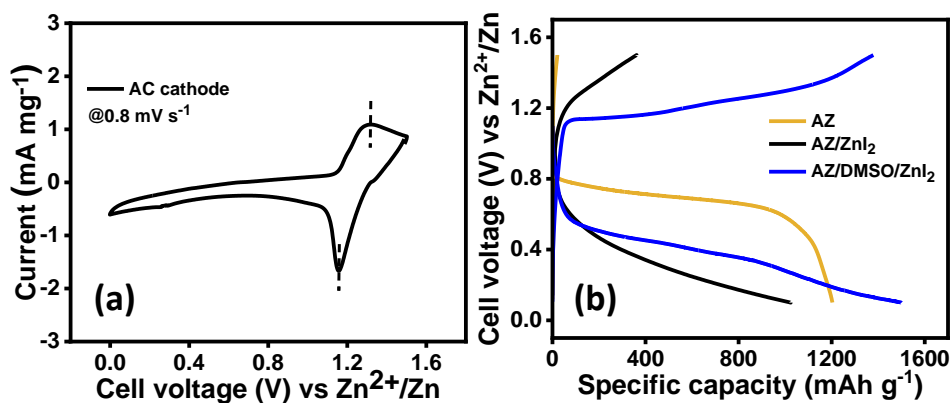


Fig. S6. (a) CV curves of the Zn/S batteries using AC cathode in AZ/DMSO/ZnI₂ electrolytes at 0.8 mV s⁻¹, and (b) Specific capacity plot of the battery operated with AZ, AZ/ZnI₂, and AZ/DMSO/ZnI₂ electrolytes at 0.1 A g⁻¹.

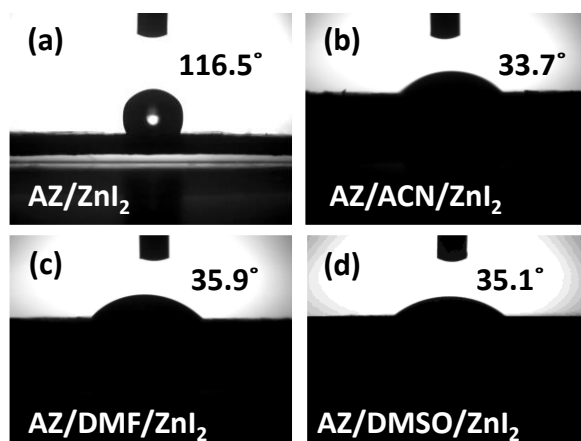


Fig. S7. WCA of (a) AZ/ZnI₂; (b) AZ/ACN/ZnI₂; (c) AZ/DMF/ZnI₂, and (d) AZ/DMSO/ZnI₂ electrolytes on sulfur cathode.

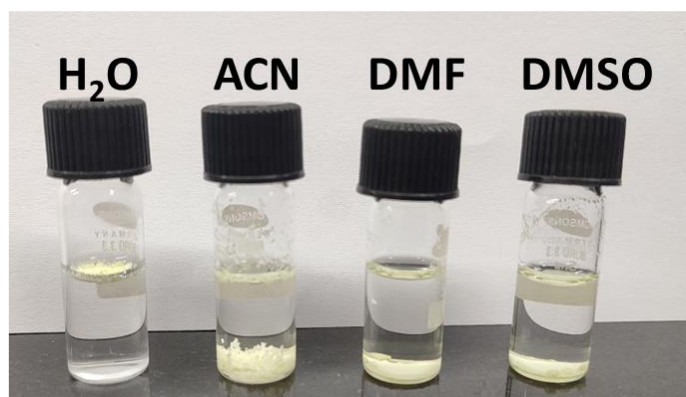


Fig. S8. Wettability of sulfur powder in water, ACN/water (40/60 v/v); DMF/water (40/60 v/v); and DMSO/water (20/80 v/v).

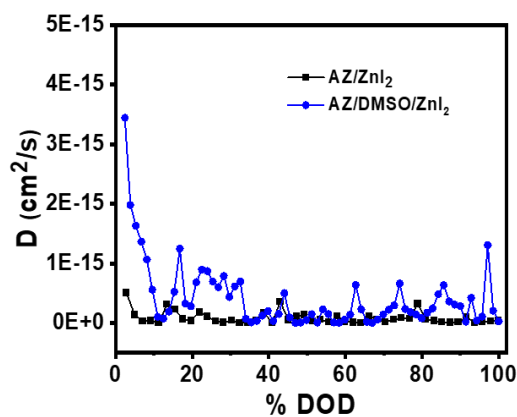


Fig. S9. Diffusion co-efficient obtained from GITT in AZ/ZnI₂ and AZ/DMSO/ZnI₂.

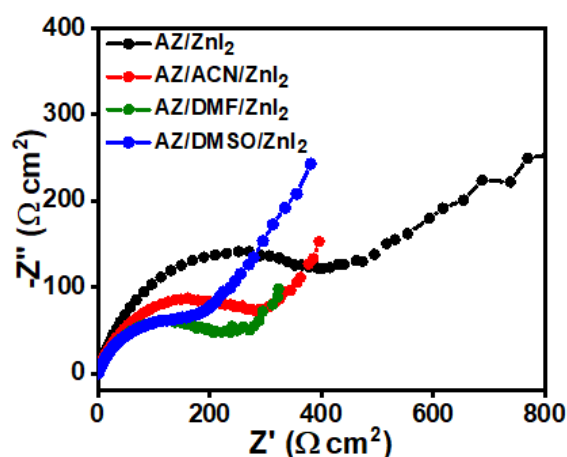


Fig. S10. EIS of Zn/S battery assembled utilizing various hybrid electrolytes.

Exchange current density for Zn/S batteries utilizing various electrolytes was calculated using the following equations:¹

$$j_0 = RT/nFAR_{ct}$$

j_0 , R , T , n , F , A , and R_{ct} represent the exchange current density, universal gas constant, temperature, number of electrons, Faraday constant, the surface area of the electrode and charge transfer resistance respectively.

Table S10. Exchange current density obtained from EIS of Zn-S batteries utilizing various hybrid electrolytes.

Electrolyte	j_0 (mA cm ⁻²)
AZ/ZnI ₂	4.46
AZ/ACN/ZnI ₂	5.37
AZ/DMF/ZnI ₂	8.81
AZ/DMSO/ZnI ₂	10.95

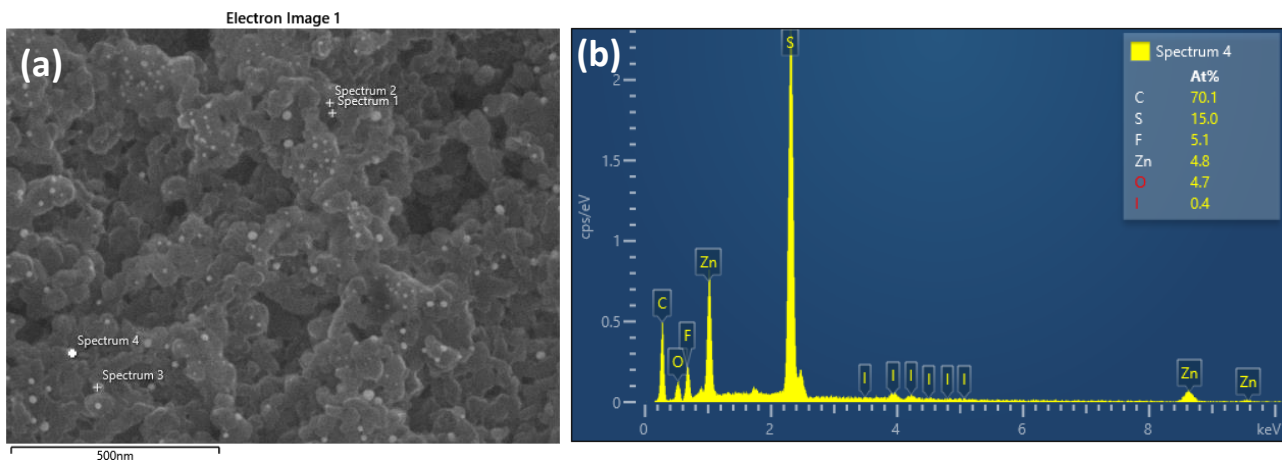


Fig. S11. (a) FESEM images of sulfur cathode after 800 cycles; and (b) Corresponding EDAX (From the position spectrum 4, other three points also show similar elemental distribution).



Fig. S12. OCP obtained by assembling two Zn/S batteries.

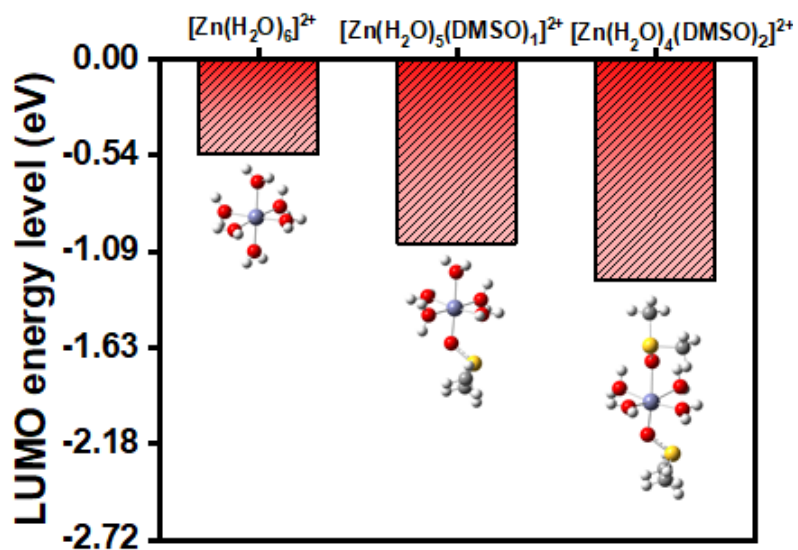


Fig. S13. LUMO energy level of $[\text{Zn}(\text{H}_2\text{O})_6]^{2+}$, $[\text{Zn}(\text{H}_2\text{O})_5(\text{DMSO})_1]^{2+}$ and $[\text{Zn}(\text{H}_2\text{O})_4(\text{DMSO})_2]^{2+}$

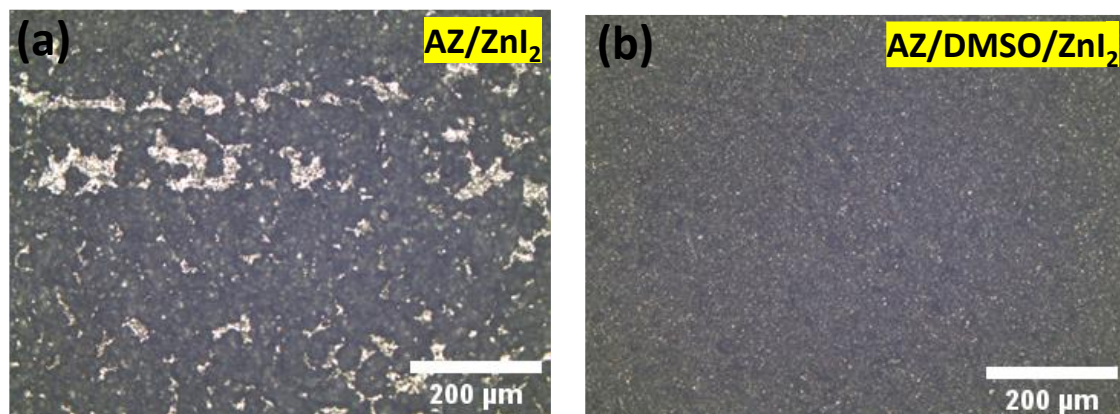


Fig. S14. Optical images of Zn in (a) AZ/ZnI₂, and (b) AZ/DMSO/ZnI₂ electrolytes after 1 h deposition time

Table S11. Performance comparison with reported Zn/S batteries.

Strategy	Anode	Cathode	Electrolyte	Initial capacity (mAh g ⁻¹)	Cycling Stability	Reference
Electrolyte additive	Zn foil	S@AC	2M Zn(OTf) ₂ + DMSO + 0.05 wt.% ZnI ₂	1502 @0.1 Ag ⁻¹	92% @5 A g ⁻¹ (1000 cycles) 62% @5 A g ⁻¹ (2000 cycles)	This work
Electrolyte additive	Zn foil	S@AC	2M Zn(OTf) ₂ + DMA + ZnI ₂	1453 @0.1 Ag ⁻¹	72% @5 A g ⁻¹ (300 cycles)	[2]
Electrolyte additive	Zn foil	S@CNTs-50	1M Zn(CH ₃ COO) ₂ + 0.05 wt.% I ₂	1105 @0.1 Ag ⁻¹	85% @1 A g ⁻¹ (50 cycles)	[3]
Electrolyte additive	Zn foil	CMK-3@S	3M Zn(OTf) ₂ + 0.1 wt.% I ₂	788 @0.2 Ag ⁻¹	90% @1 A g ⁻¹ (200 cycles)	[4]
Electrolyte additive	Zn foil	S@C	Zn(OTf) ₂ /PM/ZnI ₂	1456 @0.2 A g ⁻¹	70% @ 3 A g ⁻¹ (1200 cycles)	[5]
Electrolyte additive	Zn plate	S@CNTs-50	1m Zn(CH ₃ COO) ₂ + PEG-400	1116 @0.1 Ag ⁻¹	-	[6]
Electrolyte additive	Zn foil	S@carbon sphere	Succinonitrile+ 8 M Zn(ClO ₄) ₂	1284 @0.1 A g ⁻¹	85.7% @2A g ⁻¹ (500 cycles)	[7]
Electrolyte additive	Zn foil	HCS/S-53.7	2M Zn(OTf) ₂ + 40% Tetraglyme +0.15 wt.% I ₂	1140 @0.5 Ag ⁻¹	70% @4 A g ⁻¹ (600 cycles)	[8]
Electrolyte additive	Zn foil	S@NPC	2M Zn(OTf) ₂ +Ethylene glycol +50 mM ZnI ₂	1435 @0.1 Ag ⁻¹	70% @3 A g ⁻¹ (250 cycles)	[9]
Electrolyte additive	Zn foil	ZnS@CF	3M ZnSO ₄ + 1 wt.% iodinated thiourea (TUI)	1410 @0.1 Ag ⁻¹	71% @2A g ⁻¹ (300 cycles)	[10]
Electrolyte additive	Zn foil	S@KB	1m Zn(CH ₃ COO) ₂ +Me ₃ PhN ⁺ I ⁻	1659 @0.1 Ag ⁻¹	60% @3A g ⁻¹ (100 cycles)	[11]
Electrolyte additive	Zn foil	AJPC/S	1M Zn(OTf) ₂ + DMC + I ₂	1167 @0.1 Ag ⁻¹	47.6% @1A g ⁻¹ (200 cycles)	[12]
Electrolyte	Zn foil	S@C	1M ZnCl ₂ + D-Zn-Li 5%AN	846 @0.5 Ag ⁻¹	21% @1A g ⁻¹ (400 cycles)	[13]

Electrolyte	Zn foil	CNF-S	1M Zn(CH ₃ COO) ₂ . I ₂ /W-EG	511 @1 Ag ⁻¹	39.7% @1A g ⁻¹ (500 cycles)	[14]
Electrolyte	Zn foil	S@VC	Zn(OAc) ₂ -I ₂ -EG(10%)	1210 @0.1 C	91% @1C (250 cycles)	[15]
Electrolyte	Zn foil	S@AC-3000	1M Zn(OTf) ₂ +1M LiTFSI+ TMS + I ₂	799 @2 Ag ⁻¹	82% @2.8A g ⁻¹ (200 cycles)	[16]
Cathode	Zn foil	S@Fe-PANi	2M ZnSO ₄	1205 @0.2 Ag ⁻¹	54% @1A g ⁻¹ (200 cycles)	[17]
Cathode	Zn foil	S@FeNC/NC/CC	2M ZnSO ₄	1143 @0.2 Ag ⁻¹	57.7% @0.5A g ⁻¹ (300 cycles)	[18]
Cathode	Zn sheet	Te ₁ S ₇ /C	1M ZnSO ₄ + TEGDME	1335 @0.1 Ag ⁻¹	91.3% @0.2A g ⁻¹ (10 cycles)	[19]
Cathode	Zn foil	(poly(Li ₂ S ₆ -rDIB)copolymer	1M Zn(TFSI) ₂ + 21M LiTFSI	1148 @0.3 Ag ⁻¹	-	[20]
Cathode	Zn foil	S@S,N-CNF	3M ZnSO ₄ +75 Mm ZnI ₂	1481 @0.5 Ag ⁻¹	-	[21]
Anode	powder-Zn/indium (pZn/In)	CMK-3/S	2M ZnSO ₄ + 20 mM ZnI ₂	803 @2C	49% @2C (100 cycles)	[22]

References:

1. T. Swamy and Y.-M. Chiang, *J. Electrochem. Soc.*, 2015, **162**, A7129.
2. T. S. Thomas, A. P. Sinha and D. Mandal, *J. Mater. Chem. A*, 2024, **12**, 21350-21356.
3. W. Li, K. Wang and K. Jiang, *Adv. Sci.*, 2020, **7**, 2000761.
4. Z. Xu, Y. Zhang, W. Gou, M. Liu, Y. Sun, X. Han, W. Sun and C. Li, *Chem. Commun.*, 2022, **58**, 8145-8148.
5. Y. Guo, X. Zhu, J. Zhang, T. Zhang, Z. Wang, M. Shan, F. Wang, C. C. Cao, G. Xu and M. Zhu, *Angew. Chem. Int. Ed.*, 2024, **64**, e202422047.
6. T. Zhou, H. Wan, M. Liu, Q. Wu, Z. Fan and Y. Zhu, *Mater. Today Energy*, 2022, **27**, 101025.
7. Z. Chen, Z. Huang, J. Zhu, D. Li, A. Chen, Z. Wei, Y. Wang, N. Li and C. Zhi, *Adv. Mater.*, 2024, **36**, 2402898.
8. M. Yang, Z. Yan, J. Xiao, W. Xin, L. Zhang, H. Peng, Y. Geng, J. Li, Y. Wang, L. Liu and Z. Zhu, *Angew. Chem. Int. Ed.*, 2022, **61**, e202212666.
9. Y. Guo, R. Chua, Y. Chen, Y. Cai, E. J. J. Tang, J. J. N. Lim, T. H. Tran, V. Verma, M. W. Wong and M. Srinivasan, *Small*, 2023, **19**, 2207133.
10. D. Liu, B. He, Y. Zhong, J. Chen, L. Yuan, Z. Li and Y. Huang, *Nano Energy*, 2022, **101**, 107474.
11. W. Wu, S. Wang, L. Lin, H.-Y. Shi and X. Sun, *Energy Environ. Sci.*, 2023, **16**, 4326-4333.
12. D. Patel, A. Dharmesh, Y. Sharma, P. Rani and A. K. Sharma, *Chem. Eng. J.*, 2024, **479**, 147722.
13. M. Cui, J. Fei, F. Mo, H. Lei and Y. Huang, *ACS Appl. Mater. Interfaces*, 2021, **13**, 54981-54989.
14. A. Amiri, R. Sellers, M. Naraghi and A. A. Polycarpou, *ACS Nano*, 2023, **17**, 1217-1228.
15. S. Mehta, S. Kaur, M. Singh, M. Kumar, K. Kumar, S. K. Meena and T. C. Nagaiah, *Advanced Energy Materials*, 2024, **14**, 2401515.
16. S. Shen, C. Yuan, Y. Xu, Y. Xie, L. Wang, T. Yan, S. Chen, L. Wang, T. Liu and L. Zhang, *Adv. Funct. Mater.*, 2024, 2420258.
17. H. Zhang, Z. Shang, G. Luo, S. Jiao, R. Cao, Q. Chen and K. Lu, *ACS Nano*, 2022, **16**, 7344-7351.
18. W. Zhang, M. Wang, J. Ma, H. Zhang, L. Fu, B. Song, S. Lu and K. Lu, *Adv. Funct. Mater.*, 2023, **33**, 2210899.
19. Y. Zhang, A. Amardeep, Z. Wu, L. Tao, J. Xu, D. J. Freschi and J. Liu, *Adv. Sci.*, 2024, **11**, 2308580.
20. Y. Zhao, D. Wang, X. Li, Q. Yang, Y. Guo, F. Mo, Q. Li, C. Peng, H. Li and C. Zhi, *Adv. Mater.*, 2020, **32**, 2003070.
21. J. Li, J. Liu, F. Xie, R. Bi and L. Zhang, *Angew. Chem. Int. Ed.*, 2024, **63**, e202406126.
22. J. Li, Z. Cheng, Z. Li and Y. Huang, *Mater. Horiz.*, 2023, **10**, 2436-2444.